Tensor analyzing powers for ^{7}Li breakup

N. J. Davis, C. H. Shepherd-Themistocleous,* A. C. Shotter, T. Davinson, D. G. Ireland,† K. Livingston,† E. W. Macdonald,‡ R. D. Page,§ P. J. Sellin,‖ and P. J. Woods
Department of Physics and Astronomy, University of Edinburgh, Mayfield Road, Edinburgh EH9 3JZ, Scotland

N. M. Clarke, G. Tungate, J. A. R. Griffith, S. J. Hall, O. Karban,¶ I. Martel-Bravo,** and J. M. Nelson
School of Physics and Space Research, University of Birmingham, Edgbaston, Birmingham B15 2TT, England

K. Rusek
Soltan Institute for Nuclear Studies, Zaklad 1, Hoza 69, 00 681 Warsaw, Poland

J. Gómez-Camacho
Departmento de FAMN, Facultad de Fisicas, Universidad de Sevilla, Aptdo. 1065, 41080 Sevilla, Spain
(Received 5 July 1995)

Differential cross sections and T_{20} and $^7T_{20}$ analyzing powers have been measured for 70 MeV ^{7}Li breakup into the α particle plus triton channel, on a ^{120}Sn target. Measurements were made for both continuum breakup and sequential breakup via the 4.63 MeV state in ^{7}Li. The T_{20} data for the continuum breakup do not agree with a semiclassical Coulomb model, indicating that the breakup at small angles does not proceed solely via a Coulomb force. The data generally show a somewhat better agreement with continuum discretized coupled channels calculations, indicating the importance of the nuclear force and channel coupling in the reaction mechanism.

PACS number(s): 25.70.Mn, 24.10.Eq, 24.70.+s

I. INTRODUCTION

The α plus triton cluster structure of ^{7}Li results in a large breakup yield to these fragments. A detailed study of the breakup is of interest because two mechanisms have been observed [1–3], sequential breakup following excitation of the ^{7}Li, in particular to the 4.63 MeV $7/2^-$ state, and breakup into the α particle plus triton energy continuum.

In addition to the nuclear physics interest, breakup reactions may also be used to infer low energy photocapture cross sections necessary for an understanding of the creation of ^{7}Li in the big bang standard model. It is difficult to obtain the photocapture data directly at the low relative energies which are most important because Coulomb repulsion between the α particle and the triton results in very small cross sections. A Coulomb breakup reaction may be used instead, but it is essential to determine the importance of the nuclear force in the reaction mechanism, as any contribution from it may invalidate the inference of photocapture cross sections [4].

The continuum breakup yield is strong at forward angles and falls off rapidly at larger angles [2]. The continuum breakup can be explained by the differential strong nuclear force between the target and fragments [5], in an α particle plus triton cluster description of ^{7}Li. However, the Coulomb force becomes important at extreme forward angles [6].

Differential cross sections for the ^{7}Li continuum breakup on a ^{120}Sn target have previously been measured and found to agree at small angles with a calculation which assumes a pure Coulomb force [2,3,6,7]. The cross sections are calculated using a semiclassical approximation [8] in which the motion of the projectile along a hyperbolic trajectory is parametrized in the framework of first order perturbation theory by dimensionless orbital integrals. In order to determine the differential cross section the reduced transition probability as a function of relative energy is required. This may be obtained [9] from data on the inverse fusion reaction [10]. Thus the semiclassical Coulomb calculations of differential cross section require input based on other experimental data. Semiclassical calculations of analyzing powers, however, do not rely on additional experimental data. This is because the reduced transition probability is independent of spin substate and therefore cancels. Semiclassical Coulomb calculations have been successfully applied to ^{7}Li elastic and quasielastic scattering T_{20} analyzing powers [11]. In the current work semiclassical Coulomb calcualtions are developed for breakup analyzing powers. The analyzing powers may be more sensitive to contributions from different forces than the differential cross section because they depend on interference terms between scattering amplitudes. A comparison of calculations with the data therefore provides an additional test of the importance of the different forces. In particular, if the Coulomb force dominates, deviation of the continuum

*Present address: CERN, CH-1211, Geneva, Switzerland.
†Present address: Department of Physics, University of Glasgow, Glasgow, UK.
‡Present address: General Accident Insurance, Perth, UK.
§Present address: Department of Physics, University of Liverpool, Liverpool, UK.
‖Present address: Department of Physics, University of Sheffield, Sheffield, UK.
¶Present address: Velice 26, 37351 Driten Czech Republic.
**Present address: Departmento de FAMN, Facultad de Fisicas, Universidad de Sevilla, Aptdo. 1065, 41080 Sevilla, Spain.

breakup data from the semiclassical Coulomb calculations could occur for even a small contribution from the nuclear force in the breakup reaction mechanism.

Continuum discretized coupled channels (CDCC) calculations, which include a nuclear force, may also be performed to compare with the data. Such calculations have been found to provide a very good description of cross sections and analyzing powers for elastic and inelastic scattering of ^{7}Li [12–14]. CDCC calculations, involving a nuclear force only, have previously been compared with differential cross sections for ^{7}Li continuum and sequential breakup on a ^{120}Sn target [12]. Reasonable agreement was obtained except at the forward angles. An investigation of the effect of the Coulomb force on the sequential breakup was performed by including a Coulomb interaction derived by folding the Coulomb potential between a nucleon and the target with the transition densities between ^{7}Li states. The Coulomb force was found to contribute significantly at forward angles. A similar investigation of the effect of the Coulomb force on the continuum breakup was not, however, performed. In the current work CDCC calculations are applied to breakup analyzing powers, providing a very important new test of the CDCC approach.

Any breakup process resulting in two fragments is a three-body reaction with two reaction planes defined by the incident particle and the detected fragments. Consequently the choice of coordinate system is generally not obvious, although it is important for the theoretical interpretation of the data that it be as simple as possible, particularly when polarization effects are involved. Clearly the simplest situation corresponds to an experimental arrangement when the two reaction planes nearly coincide (see Sec. IV) and a standard two-body reaction coordinate system can be defined. It should be explained that in the semiclassical and CDCC calculations the underlying three-body reaction is interpreted by means of a two-body reaction. In order to do this assumptions about the basic reaction mechanism have to be made. These are that the incident ^{7}Li with spin $s=3/2$ and projection α is excited to a continuum or resonant state characterised by spin s' and projection γ and that this decays spatially into an α particle and a triton with a relative angular momentum L, where $\mathbf{L}+1/2=\mathbf{s}'$, and a substate m_L, where $m_L+m_t=\gamma$ and m_t is the triton spin substate. Only in the case of $L=0$, when the breakup is isotropic, can the analyzing powers calculated by either inelastic scattering theory be compared directly with the experimental data. Generally, the measured analyzing powers have to be compared with predicted quantities involving polarization transfer coefficients and correlation functions (see Sec. III).

The aim of the current work is a measurement of the T_{20} and $^TT_{20}$ analyzing powers for ^{7}Li breakup, in order to determine the importance of the Coulomb and nuclear forces in the continuum breakup reaction mechanism and investigate the applicability of semiclassical and CDCC calculations.

II. SEMICLASSICAL COULOMB CALCULATIONS

A. General formalism

Analyzing powers may be expressed in terms of scattering amplitudes $F^{\alpha\beta}_{\gamma\delta}$ where β and δ are the spin substates for the target and residual nucleus. The analyzing powers are given by [15]

$$T_{kq}=\frac{\Sigma_{\alpha\alpha'\beta\gamma\delta}\hat{s}\hat{k}(-1)^{s-\alpha-q}\begin{pmatrix} s & s & k \\ \alpha' & -\alpha & -q\end{pmatrix}F^{\alpha\beta *}_{\gamma\delta}F^{\alpha'\beta}_{\gamma\delta}}{\Sigma_{\alpha\beta\gamma\delta}|F^{\alpha\beta}_{\gamma\delta}|^2}, \tag{1}$$

where $\alpha'=\alpha+q$ and the usual notation $\hat{k}=\sqrt{2k+1}$ is used. For a spin zero target and residual nucleus, this expression is simplified because $\beta=\delta=0$.

If the motion and Coulomb interaction between the projectile and target can be described semiclassically, it may be parametrized in the framework of first order perturbation theory by dimensionless orbital integrals $R_{\lambda\mu}(\theta,\zeta)$ [8]. The potential used in the time-dependent Schrödinger equation for the particle motion may be expanded in terms of components for different multipoles λ with projections μ. The orbital integrals are related to the coefficients of this expansion and depend only on the scattering angle θ and the dimensionless adiabaticity parameter ζ. The latter depends on the energy E of the transition and the beam energy E_B if both are in units of MeV by

$$\zeta=\frac{Z_pZ_tA_p^{1/2}E}{12.7E_B^{3/2}}\left(1+\frac{A_p}{A_t}\right), \tag{2}$$

where Z is the atomic number, A is the mass number, and the suffixes p and t indicate projectile and target, respectively. Using the semiclassical approach, the scattering amplitude for Coulomb excitation to a state with spin s', may be expressed in terms of the orbital integrals by [16]

$$F^{\alpha}_{\gamma}=-i(-1)^{s-\alpha}\hat{\lambda}\begin{pmatrix} s & \lambda & s' \\ -\alpha & \mu & \gamma\end{pmatrix}\chi^{\lambda}_{s\to s'}R_{\lambda\mu}(\theta,\zeta), \tag{3}$$

where $\chi^{\lambda}_{s\to s'}$ is the strength parameter for multipole excitation of order λ to a final ejectile state of spin s'. The target remains in its ground state. Substituting Eq. (3) into Eq. (1) gives

$$T_{kq}=\frac{\hat{\lambda}^2\hat{s}\hat{k}\Sigma_{\alpha\mu}(-1)^{s-\alpha}\begin{pmatrix} s & s & k \\ \alpha+q & -\alpha & -q\end{pmatrix}\begin{pmatrix} s & \lambda & s' \\ -\alpha & \mu & \alpha-\mu\end{pmatrix}\begin{pmatrix} s & \lambda & s' \\ -\alpha-q & \mu+q & \alpha-\mu\end{pmatrix}R^*_{\lambda\mu}R_{\lambda\mu'}}{\Sigma_{\mu}|R_{\lambda\mu}|^2}, \tag{4}$$

where $\mu' = \mu + q$ and the (θ, ζ) dependence of the orbital integrals has been omitted for the sake of brevity. The strength parameter is independent of spin substate and therefore cancels in the expression for the analyzing powers. The analyzing powers for a Coulomb process consequently depend only on the initial and final spins, the multipole of the transition, and the orbital integrals.

B. Application to ^{7}Li continuum breakup

For application of the calculations to the continuum breakup of ^{7}Li into the α particle plus triton channel, the relative motion of the fragments must be assumed to have a single angular momentum. The most significant Coulomb multipole term leading to breakup is an $E1$ transition, corresponding to $L=0$ and leading to an α particle plus triton final state which has spin parity $1/2^+$. Therefore $s=3/2$, $s'=1/2$, and $\lambda=1$. Using Eq. (4) the second rank analyzing powers are calculated in terms of the orbital integrals as

$$T_{20}=\frac{|R_{11}|^2+|R_{1-1}|^2-2|R_{10}|^2}{2(|R_{11}|^2+|R_{1-1}|^2+|R_{10}|^2)}, \tag{5}$$

$$T_{21}=\frac{\sqrt{3}(R^*_{1-1}R_{10}-R_{11}R^*_{10})}{2(|R_{11}|^2+|R_{1-1}|^2+|R_{10}|^2)}, \tag{6}$$

$$T_{22}=\frac{\sqrt{3}R_{11}R^*_{1-1}}{\sqrt{2}(|R_{11}|^2+|R_{1-1}|^2+|R_{10}|^2)}. \tag{7}$$

In order to proceed further with the analyzing power calculations, expressions must be found for the orbital integrals; these are coordinate system dependent. The helicity coordinate system [17], H, was used for the T_{20} measurements. However, orbital integrals are more readily calculated in a coordinate system [8], A, with the z axis normal to the reaction plane and the x axis bisecting incident, $\mathbf{k}_{\text{in}}$, and outgoing, $\mathbf{k}_{\text{out}}$, wave vectors. The coordinate systems A and H are shown in Fig. 1. Analyzing powers in H may be determined by first calculating them in A and then rotating to H.

The orbital integrals in A can be expressed in terms of Coulomb excitation functions [8] $I_{\lambda\mu}$, which are real and coordinate system independent, such that

$$R^A_{1\pm1}=\frac{\mp I_{1\pm1}}{2\sqrt{2}}, \tag{8}$$

$$R^A_{10}=0. \tag{9}$$

Substituting Eqs. (8) and (9) into Eqs. (5) and (7) gives second rank analyzing powers in coordinate system A:

$$T^A_{20}=\frac{1}{2}, \tag{10}$$

$$T^A_{22}=\frac{-\sqrt{3}I_{11}I_{1-1}}{\sqrt{2}(I^2_{11}+I^2_{1-1})}. \tag{11}$$

Analyzing powers are spherical tensors which transform in a simple manner [18] under rotations. Thus the T_{20} analyzing power in coordinate system H may be expressed in terms of the second rank analyzing powers in coordinate system A as

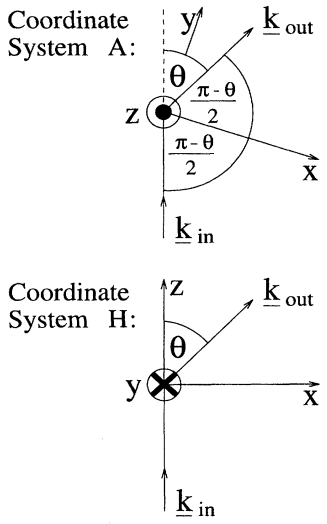

FIG. 1. Coordinate systems A and H used in the semiclassical Coulomb calculations of analyzing powers.

$$T_{20}=\sum_{q=-2,2} T^A_{2q}D^{(2)}_{q0}\left(\frac{\pi+\theta}{2},\frac{\pi}{2},\frac{3\pi}{2}\right), \tag{12}$$

where the rotation matrix elements $D^{(2)}_{q0}((\pi+\theta)/2, \pi/2, 3\pi/2)$ are functions of the Euler angles [19] for the rotation. It should be noted that the general property of analyzing powers [15],

$$T_{k-q}=(-1)^q T^*_{kq}, \tag{13}$$

results in

$$T^A_{2-2}=T^A_{22}, \tag{14}$$

and consequently Eq. (12) becomes

$$T_{20}=\frac{-[T^A_{20}+\sqrt{6}T^A_{22}\cos(\theta)]}{2}. \tag{15}$$

Substituting Eqs. (10) and (11) into Eq. (15) gives

$$T_{20}=\frac{6I_{11}I_{1-1}\cos(\theta)-I^2_{11}-I^2_{1-1}}{4(I^2_{11}+I^2_{1-1})}. \tag{16}$$

$^TT_{20}$ is simply T_{20} referred to an axis normal to the reaction plane [20]. Consequently $^TT_{20}=T^A_{20}$, and so $^TT_{20}$ is given by Eq. (10).

In order to calculate angular distributions of T_{20} the Coulomb excitation functions must be calculated. This cannot be done analytically but may be done numerically [21]. Values of the adiabaticity parameter, determined from Eq. (2), are used in the calculations. For 70 MeV ^{7}Li beam on a ^{120}Sn target, $Z_p=3$, $Z_t=50$, $A_p=7$, $A_t=120$, and $E_p=70$ in Eq. (2). E may take a range of values from 2.47, the breakup threshold in MeV, upwards, and so calculations may be performed using different adiabaticity parameters corresponding

TABLE I. Woods-Saxon optical potential parameters used in the CDCC calculations. r and a indicate radius and diffuseness parameters respectively and suffices r, i, and C indicate real, imaginary, and Coulomb potentials, respectively. V is the real potential depth and W and W_d are imaginary and derivative imaginary potentials, respectively.

	V (MeV)	r_r (fm)	a_r (fm)	W (MeV)	W_d (MeV)	r_i (fm)	a_i (fm)	r_C (fm)
$\alpha+^{120}$Sn [a]	58.0	1.46	0.708	28.0	0.0	1.46	0.708	1.4
$t+^{120}$Sn [b]	145.0	1.25	0.690	0.0	27.5	1.11	0.920	1.4
^{7}Li$=t+\alpha$	90[c]	1.39	0.700					1.3

[a]C. M. Perey and F. G. Perey, At. Data Nucl. Data Tables **17**, 1 (1976).
[b]R. P. Ward and P. R. Hayes, At. Data Nucl. Data Tables **49**, 315 (1991).
[c]For bound states the potential depth was adjusted in order to obtain the correct binding energy.

to different fragment relative energies. The analyzing powers are then determined by using the calculated Coulomb excitation functions in Eq. (16).

III. CONTINUUM DISCRETIZED COUPLED CHANNELS CALCULATIONS

The CDCC calculations were performed using the computer code FRESCO [22]. Cluster folding potentials were incorporated. The Coulomb as well as the nuclear interaction was included in the CDCC calculations. Both diagonal potentials and coupling interactions were taken into account. The nuclear and Coulomb potentials were obtained using the same method, by folding potentials between α particle cluster and target and between triton cluster and target. The potentials for the channel coupling are derived from empirical optical model potentials for a ^{120}Sn target. These are Woods-Saxon in shape and are listed in Table I. Ideally the potentials should be for 40 MeV α particles [23], as is used, and 30 MeV tritons, to correspond to beam velocity fragments from 70 MeV ^{7}Li breakup. However a 20 MeV triton potential [24] was adopted because none was available at 30 MeV.

The ^{7}Li $3/2^-$ ground state and $1/2^-$ first excited state cluster wave functions were calculated in a Woods-Saxon potential well having geometry parameters as listed in Table I. These were chosen so as to reproduce the empirical value of the reduced transition probability $B(E2;3/2^-\rightarrow 1/2^-)$ [25]. The wave function of the $7/2^-$ second excited state was calculated using a weak binding energy approximation [26], in which a very small binding energy is assumed for this state. The $5/2^-$ third excited state was treated as an energy bin of 5 MeV width.

Test calculations were performed in order to establish the best discretization and truncation of the model space. The ^{7}Li continuum was initially discretized as in a previous CDCC study by Sakuragi *et al.* [12], with values of the relative orbital angular momentum L for the $\alpha+t$ clusters limited to $L=1,3$. The test calculations were performed for the ^{7}Li$+^{208}$Pb system since experimental data for the elastic, inelastic, and breakup channels exist for this system [1,6]. Four channel calculations, including the ground state and the first three excited states, produced an angular distribution of the differential cross section for the $7/2^-$ state similar in shape to the calculations performed by Sakuragi *et al.* [12], but of about 30% lower magnitude. This may be because the latter were performed with double folding potentials. The inclusion of the nonresonant continuum reduced this by less than 10%.

The test calculations revealed that the influence of the wave number $k=(0.75-1.00)$ fm^{-1} bin on the final results is very small and that the model space can in fact be limited to the range $k=(0.25-0.75)$ fm^{-1}. The results for the lowest bin $k=(0.00-0.25)$ fm^{-1} underestimated the experimental values [1] especially at the most forward angles. This energy range was dominated by the bin with $L=1$ and spin parity $I^\pi=3/2^-$. Sakuragi *et al.* [12] argued that the coupling to the even L breakup states must be much weaker than to the odd L states and therefore the L values can be restricted to $L=1,3$. In order to investigate this further, the $L=0$ bins were included in the calculations. It was found that, although the results for the elastic and inelastic scattering and for the $7/2^-$ state were not affected by the inclusion of the $L=0$ states, the cross section calculated for the lowest $L=0$, $k=(0.00-0.25)$ fm^{-1}, continuum bin was large at scattering angles ranging from 10° to 35°. It overestimated the measured [1] values. The large cross section for the $L=0$ bin is in agreement with radiative capture studies [27] which revealed that $E1$ contributions dominate. The same was shown in an analysis of 63 MeV breakup data [28]. It was therefore considered important to include even L breakup states in the CDCC calculations, especially because the forward angle data are of particular interest. The argument by Sakuragi *et al.* [12] for neglecting even L relies on a three-body model of α particle, triton, and target in which the α particle and triton potentials with respect to the target are similar. In the present study the α particle and triton optical potentials used are very different, which may explain the large $L=0$ cross section.

CDCC calculations for 70 MeV ^{7}Li breakup on ^{120}Sn were performed using the model space shown in Fig. 2. The width of the lowest bin was set to 0.38 fm^{-1} to correspond to the continuum breakup data measured in the experiment. The model space was truncated to a maximum of 0.8 fm^{-1} and to $L=0,1,2,3$. For $L=2$, only the lowest $k=(0.0-0.38)$ fm^{-1} bin was taken into account, in order to reduce the number of channels. This limitation is not expected to significantly affect the analysis, since calculated continuum cross sections were generally found to decrease with increasing relative energy. For a comparison with the continuum breakup data it was necessary to sum the contributions of the calculations

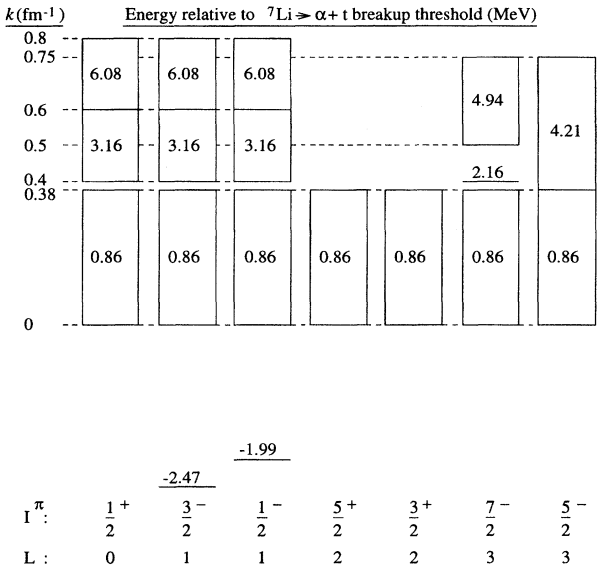

FIG. 2. The discretization of the ^{7}Li$=\alpha+t$ breakup continuum used in the coupled channels calculations.

for different spin parity values to obtain totals for the differential cross section and analyzing powers. An incoherent summation over the contributions was taken and analyzing power contributions were weighted by the corresponding differential cross sections. In order to investigate the roles of the nuclear and Coulomb forces in the CDCC calculations, additional calculations were performed with a nuclear interaction only. It was found that, subject to limitations on the numerical integrations of the coupled equations to 40 fm and on the partial waves to $150\hbar$, the results were very similar, indicating a dominant effect of the nuclear interaction.

To achieve a CDCC result for consistent comparison with the measured analyzing powers, some consideration has to be made of the phase space detected in the experiment. For the continuum breakup, the large contribution from $L=0$ results in the phase space having little effect on the calculations; hence, results direct from the FRESCO code are compared with the data. For the $L=3$ sequential breakup, phase space is far more important. In order to take account of this, consider the scattering amplitude

$$\langle \mathbf{k}_\alpha, \mathbf{k}_t, s_t m_s | A | \mathbf{k}_i; s\alpha \rangle = \sum_\gamma \langle \mathbf{k}_\alpha, \mathbf{k}_t, s_t m_s | \mathbf{k}_{\text{c.m.}}, s'\gamma \rangle A^\alpha_\gamma , \tag{17}$$

where the

$$A^\alpha_\gamma = \langle \mathbf{k}_{\text{c.m.}}, s'\gamma | A | \mathbf{k}_i, s\alpha \rangle \tag{18}$$

are amplitudes calculated by the FRESCO code, s_t and m_s are the spin and projection for the triton, $\mathbf{k}_\alpha$, $\mathbf{k}_t$, and $\mathbf{k}_i$ are the α particle, triton, and incident momenta, respectively, A is an appropriate form factor, and

$$\mathbf{k}_{\text{c.m.}} = \mathbf{k}_\alpha + \mathbf{k}_t . \tag{19}$$

Equation (17) may be written in terms of a sum over spherical harmonics of the breakup angular momentum $L=3$, projection m_L:

$$\langle \mathbf{k}_\alpha, \mathbf{k}_t, s_t m_s | A | \mathbf{k}_i; s\alpha \rangle = \sum_\gamma A^\alpha_\gamma \sum_{m_L} \langle s_t m_s L m_L | s'\gamma \rangle Y_{Lm_L}(\hat{\mathbf{k}}_r), \tag{20}$$

where

$$\mathbf{k}_r = \frac{4\mathbf{k}_t - 3\mathbf{k}_\alpha}{7} . \tag{21}$$

This relative momentum taken as triton relative to α particle could equally well be taken as α particle relative to triton.

In order to calculate appropriate analyzing powers from the scattering amplitudes, the coincidence detection probability $f(\theta_r, \phi_r)$ for fragments with relative momentum direction given by spherical polar coordinates (θ_r, ϕ_r) in the helicity coordinate system H needs to be incorporated. This probability function was calculated using a Monte Carlo simulation code [29] in which the collimator positions for the coincidence detection were defined. ^{7}Li nuclei were excited to the 4.63 MeV state with a Lorentzian distribution and were scattered isotropically over a solid angle large enough to include the collimators. The probability function $f(\theta_r, \phi_r)$ was extracted from the Monte Carlo calculation in the form of a two-dimensional spectrum of number of counts versus θ_r and ϕ_r, for which the α particle and triton were detected in coincidence. For this spectrum the θ_r range was divided into 5° bins and the ϕ_r range was divided into 10° bins. $f(\theta_r, \phi_r)$ is an even function of ϕ_r because of the symmetry of the coincidence detection system above and below the plane in which the scattering angle is defined.

The double differential cross section $d^2\sigma(\mathbf{k}_{\text{c.m.}}, \mathbf{k}_r)/d\Omega_{\text{c.m.}} d\Omega_r$ and analyzing powers T_{kq} corresponding to having the center of mass momentum of the α particle plus triton in a solid angle $\Omega_{\text{c.m.}}$ and the relative momentum in a solid angle Ω_r are given by

$$(2s+1) T_{kq} \frac{d^2\sigma(\mathbf{k}_{\text{c.m.}}, \mathbf{k}_r)}{d\Omega_{\text{c.m.}} d\Omega_r} = \frac{1}{\sqrt{4\pi}} \sum_{k'q'} X_{kq,k'q'} \hat{s}' \hat{L}^2 \begin{pmatrix} L & k' & L \\ 0 & 0 & 0 \end{pmatrix} W(LLs's'; k's_t) Y_{k'q'}(\hat{\mathbf{k}}_r), \tag{22}$$

where the polarization transfer coefficients are given by

$$X_{kq,k'q'} = \sum \langle s\alpha kq | s\alpha' \rangle \hat{k} \langle s'\gamma k'q' | s'\gamma' \rangle \hat{k}' A^\alpha_\gamma A^{\alpha'*}_{\gamma'} . \tag{23}$$

However, the experiment does not resolve in detail the double differential cross section. Instead, those relevant events where an α particle and a triton are detected in coincidence are counted as sequential breakup (SBU), which happens with the probability $f(\theta_r,\phi_r)$. Thus

$$(2s+1)T_{kq}^{\mathrm{SBU}}\frac{d\sigma^{\mathrm{SBU}}(\mathbf{k}_{\mathrm{c.m.}})}{d\Omega_{\mathrm{c.m.}}}=\int_{\phi_r=0}^{2\pi}\int_{\theta_r=0}^{\pi}f(\theta_r,\phi_r)(2s+1)T_{kq}\frac{d^2\sigma(\mathbf{k}_{\mathrm{c.m.}},\mathbf{k}_r)}{d\Omega_{\mathrm{c.m.}}d\Omega_r}\sin\theta_r d\theta_r d\phi_r$$

$$=\frac{1}{\sqrt{4\pi}}\sum_{k'q'}X_{kq,k'q'}\hat{s}'\hat{L}^2\begin{pmatrix}L & k' & L\\ 0 & 0 & 0\end{pmatrix}W(LLs's';k's_t)I_{k'q'}, \tag{24}$$

where

$$I_{k'q'}=\int_{\phi_r=0}^{2\pi}\int_{\theta_r=0}^{\pi}Y_{k'q'}(\theta_r,\phi_r)f(\theta_r,\phi_r)\sin\theta_r d\theta_r d\phi_r. \tag{25}$$

This integral is necessary because of the sensitivity of the calculated analyzing powers to the angles θ_r and ϕ_r. This is illustrated in Fig. 3, which shows analyzing powers calculated assuming single θ_r and ϕ_r values for a laboratory scattering angle of 15°. $I_{k'q'}$ reduces to a real number since $f(\theta_r,\phi_r)$ is even in ϕ_r and the integration is taken over 2π in ϕ_r. In order to calculate the analyzing powers, the integrals $I_{k'q'}$ are calculated according to Eq. (25) using the probability function $f(\theta_r,\phi_r)$ obtained from the Monte Carlo calculation and the polarization transfer coefficients $X_{kq,k'q'}$ are calculated from the FRESCO amplitudes A_γ^α according to Eq. (23). The analyzing powers are then calculated from Eq. (24), normalizing such that $T_{00}=1$.

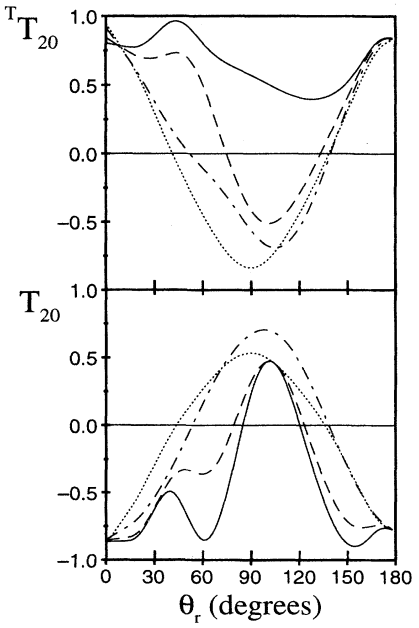

FIG. 3. CDCC calculated analyzing powers as a function of center of mass relative momentum direction, for 15° laboratory scattering angle. The solid, dashed, dot dashed, and dotted curves are for ϕ_r= 0°, 30°, 60°, and 90°, respectively.

IV. EXPERIMENT

The experiment was performed using 70 MeV polarized ^{7}Li beams from the polarized heavy ion source [30] and accelerated by the tandem Van de Graaf accelerator, at the Nuclear Structure Facility at Daresbury Laboratory in the UK. For the $^{T}T_{20}$ measurements polarization of the beam was achieved using rf transitions between the 2-8 and 4-6 hyperfine atomic levels [31] in a magnetic field, resulting in states with equal magnitude but opposite signs of the tensor polarization and equal odd rank polarizations. This equality was verified by comparison with an unpolarized beam. The T_{20} measurements were made at a later date when optical pumping [32] was available for polarization of the beam, doubling the theoretical maximum polarization obtainable. Ions with each of the four spin substates were selected in turn, using a high frequency transition in a magnetic field to switch between substates. For both T_{20} and $^{T}T_{20}$ measurements, the polarization states were switched every few seconds, after a specified integrated beam current was measured, to minimize systematic errors due to beam drift or polarization fluctuations. A Wien filter was used to orient the polarization symmetry axis along the beam direction at the target for the T_{20} measurements and normal to a plane bisecting fragment coincidence detector centers for the $^{T}T_{20}$ measurements. The beam polarization was determined from the ^{1}H(^{7}Li,α)^{4}He reaction [16] using a purpose built downstream polarimeter [33]. The measured magnitudes of second rank beam polarizations were typically t_{20}=0.4 for the $^{T}T_{20}$ measurements and t_{20}=0.6 for the T_{20} measurements. Measurements of first and third rank polarizations in the optically pumped beam resulted in magnitudes no larger than 0.05 each.

For the breakup reactions a 2 mg cm^{-2} ^{120}Sn target was used. The yield for continuum breakup of ^{7}Li into an α particle and a triton is large for small relative energies of the fragments [2]. For this reason fragments with a small opening angle must be detected. The detection system consisted of two pairs of $\Delta E\cdot E$ detector telescopes placed symmetrically, one pair either side of the beam, as shown in Fig. 4. The symmetric arrangement was used so that data from both sides of the beam could be summed, thus eliminating systematic errors arising from any shift in position of the beam on target and the effects of odd rank polarization components in the beam. The telescopes comprised of 230 μm thick p-n

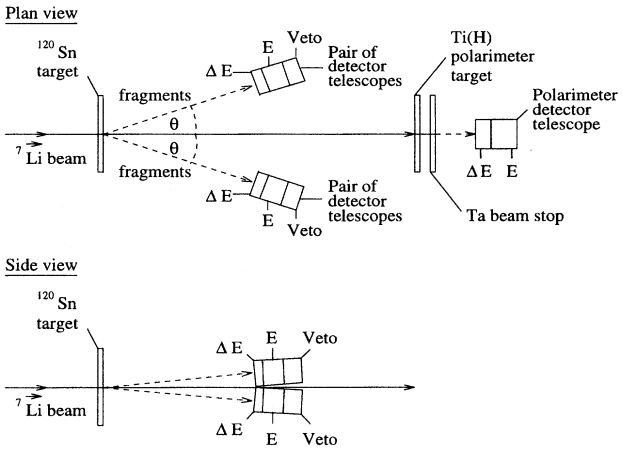

FIG. 4. Detector system.

junction silicon ΔE detectors and 4 mm thick lithium drifted silicon E detectors. Similar detectors placed behind the E detectors acted as vetos to eliminate high energy charge 1 particles which pass through the E detectors. The detector collimators were 8 mm wide and 6 mm high with the centers for a given pair 12 mm apart. The detectors in each pair of telescopes were mounted symmetrically above and below the beam axis and 150 mm from the target.

The detectors were energy calibrated using 5.486 MeV α particles from ^{241}Am sources mounted close to the detectors. Particle identification was achieved using the ΔE and E signals. Fast timing was achieved by signals generated from the ΔE preamplifiers, used to start and stop a time to amplitude converter for each pair of telescopes. Data were transmitted from analogue to digital converters to a GEC 4190 computer and recorded event by event on tape.

T_{20} and $^TT_{20}$ data were obtained for a range of angles to the beam direction, θ, shown in Fig. 4, from 9° to 25° in the laboratory frame.

V. RESULTS

The fast coincidence data were gated on the ground state of ^{120}Sn by summing triton and α particle energies. An energy resolution of 0.4 MeV was achieved. A coincidence spectrum of triton energy is shown in Fig. 5. The sharp peaks correspond to the two kinematic solutions for sequential

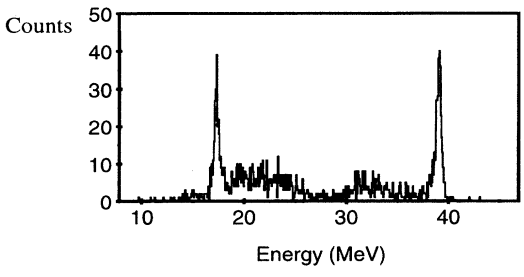

FIG. 5. Energy spectrum of tritons from the ^{120}Sn(^{7}Li,αt) ^{120}Sn$_{g.s.}$ reaction at a laboratory angle of 15°.

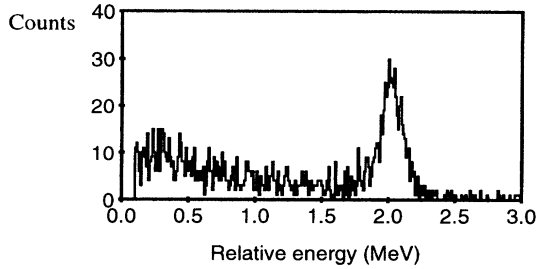

FIG. 6. Fragment relative energy spectrum for the ^{120}Sn(^{7}Li, αt) ^{120}Sn$_{g.s.}$ reaction at a laboratory angle of 15°.

breakup via the 4.63 MeV state in ^{7}Li and the data between the peaks arise from continuum breakup [2]. The relative energy ϵ between the triton and α particle may be calculated according to

$$\epsilon = \frac{4E_t + 3E_\alpha - 4\sqrt{3E_tE_\alpha}\cos(\phi)}{7}, \tag{26}$$

where E_t and E_α are the triton and α particle energies respectively and ϕ is the angle between them. Figure 6 shows a relative energy spectrum, where ϕ has been taken to be the angle between the detector collimator centres. The peak is from the sequential breakup and the data at lower relative energies are from continuum breakup. Yields were obtained for each polarization state of the beam. This enabled data for the continuum breakup to be obtained from a threshold of 100 keV to 1.7 MeV in relative energy.

The measured analyzing powers for the ^{120}Sn(^{7}Li,αt) ^{120}Sn$_{g.s.}$ continuum breakup are compared with semiclassical Coulomb and CDCC calculations in Fig. 7. The small relative energy dependence of the semiclassical Coulomb calculations of T_{20} is shown by the dashed curve which corresponds to zero relative energy and the dotted curve which corresponds to a relative energy of 2.16 MeV, equivalent to the value for sequential breakup via the 4.63 MeV state in ^{7}Li. The corresponding calculation of $^TT_{20}$ is not relative energy dependent and is shown by the dashed curve. The $^TT_{20}$ data agree well with the semiclassical calculation at small angles but deviate from it at the larger angles. The T_{20} data clearly do not agree with these calculations. The angular trend of the data opposes that of the calculations and large magnitude T_{20} values are measured, in disagreement with the small magnitudes predicted by the calculations. This result is in contrast with the results of differential cross section [2,3,6] measurements which indicated that the Coulomb force is responsible for the continuum breakup at small angles. Analyzing powers are more sensitive than differential cross sections to the contributions of different forces in the reaction mechanism and thus will be affected by a nuclear force present in the reaction mechanism even if the Coulomb force also plays a large role. The extent of the disagreement between the T_{20} data and the calculations indicates, however, that the nuclear contribution to the continuum breakup is significant. The T_{20} measurement provides a more rigorous test of the semiclassical Coulomb model than the $^TT_{20}$ measurement. This is because the calculation of T_{20} depends di-

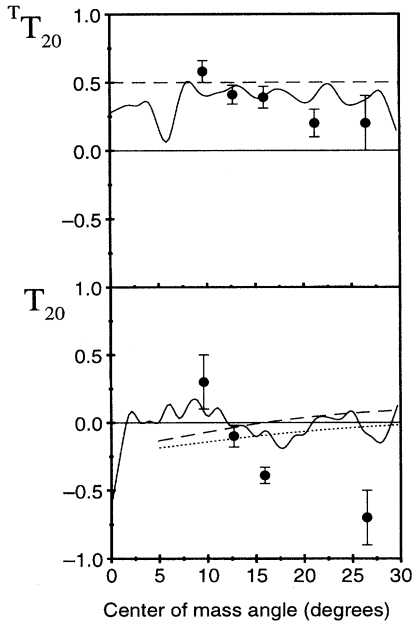

FIG. 7. T_{20} and $^{T}T_{20}$ for ^{120}Sn(^{7}Li,αt)^{120}Sn$_{g.s.}$ continuum breakup for $\epsilon \leq 1.7$ MeV. The dashed curves show semiclassical calculations for $^{T}T_{20}$ and for T_{20} with $\epsilon = 0$ MeV and the dotted curve shows the semiclassical calculation for T_{20} with $\epsilon = 2.16$ MeV. The solid curves show the CDCC calculations with all L values from 0 to 3 included.

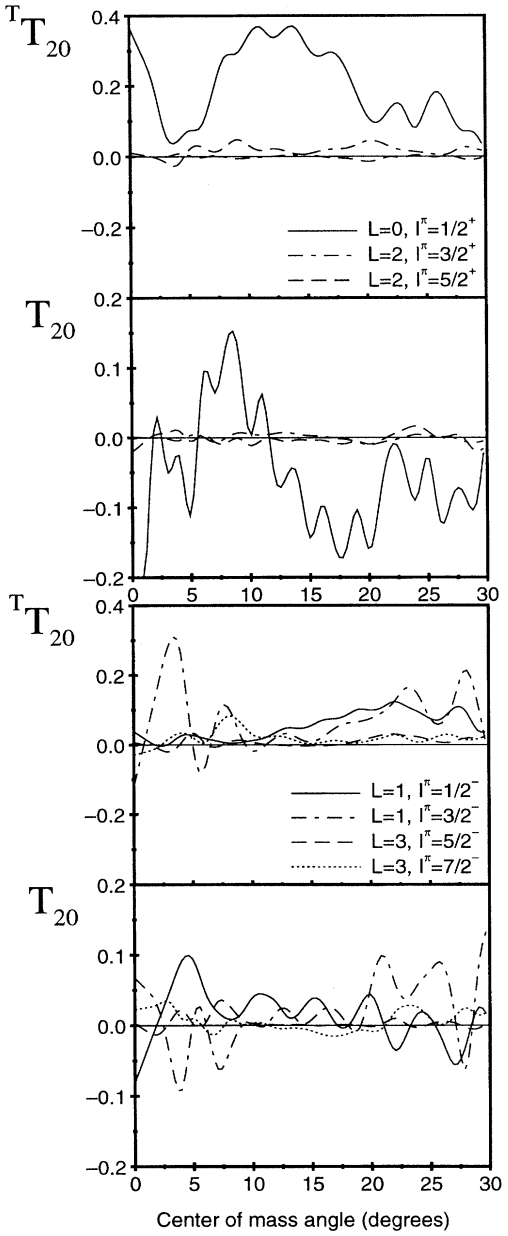

FIG. 8. CDCC calculations of T_{20} and $^{T}T_{20}$ for ^{120}Sn(^{7}Li,αt)^{120}Sn$_{g.s.}$ continuum breakup, for different L values.

rectly on the Coulomb excitation functions whereas the calculation of $^{T}T_{20}$ does not. The semiclassical calculation of $^{T}T_{20}$ only depends on the assumption of multipolarity 1, which is good for a Coulomb force but is not necessarily so for a nuclear force. Nevertheless, $^{T}T_{20}$ can not distinguish the multipolarity 1 component of a nuclear force from a Coulomb force. The T_{20} data thus expose the disagreement with the semiclassical Coulomb model better than the $^{T}T_{20}$ data. If a Coulomb force were responsible for the continuum breakup a small deviation of the data from the calculations might be expected due to the approximations used in the semiclassical model. However, the extent of the deviation for T_{20} indicates that the disagreement is more fundamental and a significant nuclear force contribution to the continuum breakup reaction mechanism is therefore expected to be present. The poor agreement of the T_{20} data with the semiclassical Coulomb calculations, observed together with the good agreement of the $^{T}T_{20}$ data with the calculations at small angles suggests that the nuclear force contribution to the continuum breakup reaction mechanism is not only significant, but also has a large multipolarity 1 component.

CDCC calculations for ^{120}Sn(^{7}Li,αt)^{120}Sn$_{g.s.}$ continuum breakup analyzing powers are shown for the different L contributions in Fig. 8. The $L=0$ contributions are the most important, because of the large associated differential cross section, with the $L=2$ and $L=3$ contributions insignificant. The $L=0$ component of the CDCC calculation of $^{T}T_{20}$ takes values between 0.4 and 0.6 over an angular range of 0°–25°, and so is very similar to the semiclassical calculation which gives a value of 0.5. The $L=1$ contributions have most effect for the larger angles, 20°–30°. The result of incoherently combining all components of the CDCC calculation gives the solid curves shown in Fig. 7. A good description of the $^{T}T_{20}$ data is obtained over the angular range measured, with the significant contribution from the $L=1$ components at larger angles enhancing agreement with the data. The CDCC and semiclassical calculations of $^{T}T_{20}$ are quite similar, with the CDCC generally a little lower than the semiclassical result of 0.5. However, the oscillations in the CDCC calculation, which are not present in the semiclassical calculation, improve the agreement with the data. The CDCC calculation is within error bars of three of the five data points while the semiclassical calculation only exhibits this quality

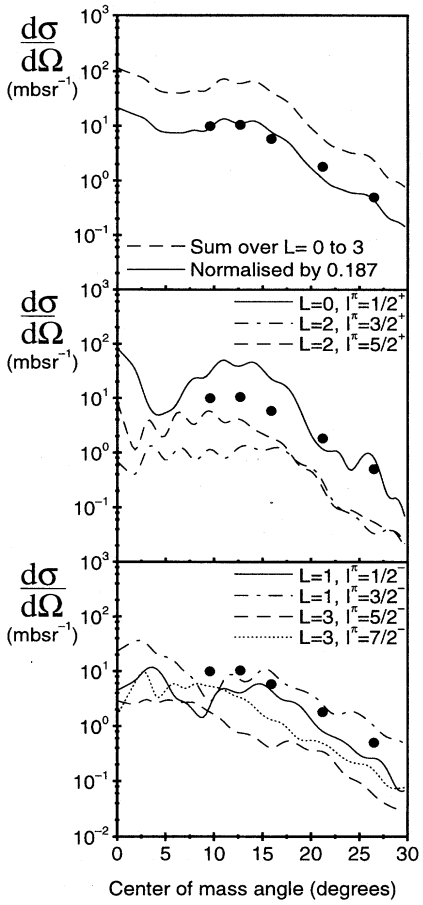

FIG. 9. Differential cross sections for ^{120}Sn(^{7}Li,αt)^{120}Sn$_{g.s.}$ continuum breakup for $\epsilon \leq 1.7$ MeV. The curves show CDCC calculations for different L values.

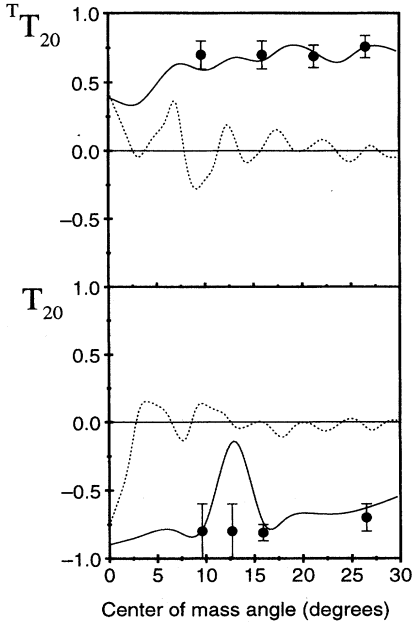

FIG. 10. T_{20} and $^TT_{20}$ for ^{120}Sn(^{7}Li,αt)^{120}Sn$_{g.s.}$ sequential breakup via the ^{7}Li 4.63 MeV state. The dotted curves show the CDCC calculations obtained directly from FRESCO and the solid curves have phase space effects included.

of agreement for the smallest angle data point. The total CDCC calculation of T_{20} shown in Fig. 7 reproduces the data at the smaller angles, largely from the $L=0$ contribution. At the larger angles where the $L=1$, $I^\pi=3/2^-$ component has a significant effect and is of opposite sign to the data, the agreement is poor. Detection phase space effects would be more important at the larger angles but are impractical to incorporate into the continuum breakup calculations. The CDCC calculation does, however, give better agreement with the small angle T_{20} data than the semiclassical Coulomb calculation does. The CDCC calculation reproduces within errors the trend between the two smallest angle data points, while the semiclassical calculation merely crosses this trend at about 12°.

It was not the aim of the experiment to measure absolute differential cross sections for the breakup and normalization difficulties prevent a reliable result. However, angular distributions of differential cross sections, for which the trend is accurate, were obtained and it is interesting to compare these with CDCC predictions. Differential cross section data for ^{120}Sn(^{7}Li,αt)^{120}Sn$_{g.s.}$ continuum breakup are compared with the results of CDCC calculations in Fig. 9. It is interesting to note that $L=0$ gives the dominant contribution to the calculated differential cross section for 7°–19°. Beyond 19° the $L=1$, $I^\pi=3/2^-$ contribution dominates. The total CDCC calculation exhibits very good agreement with the data if normalized by a factor of 0.187. There are several explanations for why this normalization is necessary. The data may have systematic uncertainties due to inaccuracies in the target thickness and in the solid angle which had to be determined by a Monte Carlo calculation [29] into which some assumption of the continuum breakup yield variation with relative energy had to be incorporated, the result of a semiclassical Coulomb calculation being used. A calculation using the FRESCO code could not reasonably be performed because of the small energy bins which would be required. Some data were also lost due to detector dead regions and electronic thresholds. The CDCC calculations may not give the correct absolute magnitude of the differential cross sections because of their cluster model basis. The agreement of the angular distribution of the CDCC calculations with the differential cross section data is, however, excellent.

Analyzing power data for ^{120}Sn(^{7}Li,αt)^{120}Sn$_{g.s.}$ sequential breakup via the 4.63 MeV state in ^{7}Li are compared with CDCC calculations in Fig. 10. The results obtained directly from the FRESCO code, shown by the dotted curves, are not sufficient to reproduce the data. However, when the phase space effects are included, as shown by the solid curves, the calculations exhibit excellent agreement with the data, with the exception of the predicted 13° maximum in T_{20} which is not seen in the data. This is most probably because the data are smeared a little over a range of angles because of finite detector sizes. The predicted maximum in T_{20} corresponds to a minimum in the differential cross section, as shown in Fig. 11. This means such smearing will have a large effect in this case, bringing the measured T_{20} towards values for nearby angles.

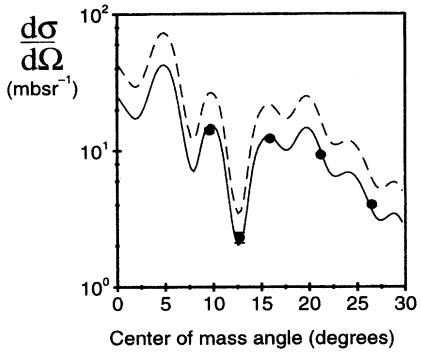

FIG. 11. Differential cross section for ^{120}Sn(^{7}Li,αt)^{120}Sn$_{g.s.}$ sequential breakup via the ^{7}Li 4.63 MeV state. The dashed curve shows the CDCC calculation and the solid curve shows the same calculation normalized by a factor of 0.584.

Differential cross section data for ^{120}Sn(^{7}Li,αt)^{120}Sn$_{g.s.}$ sequential breakup via the 4.63 MeV state in ^{7}Li are compared with the CDCC calculation in Fig. 11. As for the continuum breakup data, a normalization was found to be necessary, though in this case it can only be due to uncertainties in the target thickness and use of the cluster model in the CDCC calculation, since no relative energy dependence need be assumed in the solid angle determination. When the calculation is normalized by a factor of 0.584, as shown by the solid curve, excellent agreement with the data results. The CDCC calculation reproduces the angular distribution of the sequential breakup differential cross section, including the sharp minimum at 13°.

VI. CONCLUSIONS

Differential cross section angular distributions and T_{20} and $^{T}T_{20}$ analyzing powers have been measured for continuum and sequential breakup of 70 MeV ^{7}Li on a ^{120}Sn target.

The T_{20} data for the continuum breakup do not show agreement with semiclassical calculations which assume a pure Coulomb force, though the small angle $^{T}T_{20}$ data lie close to the calculation. This indicates that the Coulomb force is not solely responsible for the continuum breakup at small angles. For astrophysical applications, photocapture cross sections inferred from breakup data using a Coulomb force assumption may not be accurate.

CDCC calculations were found to reproduce the $^{T}T_{20}$ and small angle T_{20} data for the continuum breakup well, though agreement with the larger angle T_{20} data is not so good. It was discovered to be important to include the $L=0$ continuum contribution in the CDCC calculations. The CDCC calculation was also found to reproduce very well the angular trend of the differential cross section data for the continuum breakup. CDCC calculations which include phase space effects were found to give excellent agreement with the measured T_{20} and $^{T}T_{20}$ analyzing powers and the angular trend of the differential cross section for the sequential breakup.

ACKNOWLEDGMENTS

We would like to thank the Engineering and Physical Sciences Research Council for funding some of this project. K.L. acknowledges additional financial support from Micron Semiconductor Ltd. We are grateful to Ali El-Lithi for providing a computer code for the evaluation of Coulomb excitation functions.

[1] A.C. Shotter, A.N. Bice, J.M. Wouters, W.D. Rae, and J. Cerny, Phys. Rev. Lett. **46**, 12 (1981).
[2] A.C. Shotter, V. Rapp, T. Davinson, D. Branford, N.E. Sanderson, and M.A. Nagarajan, Phys. Rev. Lett. **53**, 1539 (1984).
[3] A.C. Shotter, V. Rapp, T. Davinson, and D. Branford, J. Phys. G **14**, L169 (1988).
[4] A.C. Shotter and M.A. Nagarajan, J. Phys. G **14**, L109 (1988).
[5] I.J. Thompson and M.A. Nagarajan, Phys. Lett. **123B**, 379 (1983).
[6] T. Davinson, V. Rapp, A.C. Shotter, D. Branford, and N.E. Sanderson, Phys. Lett. **139B**, 150 (1984).
[7] D.K. Srivastava, D.N. Basu, and H. Rebel, Phys. Lett. B **206**, 391 (1988).
[8] K. Alder and A. Winther, *Electromagnetic Excitation* (North-Holland, Amsterdam, 1975).
[9] J.M. Blatt and V.F. Weisskopf, *Theoretical Nuclear Physics* (Wiley, New York, 1952).
[10] D.F. Ottewell, Ph.D. thesis, University of Vancouver, 1976.
[11] G. Grawert and J.C. Derner, Nucl. Phys. **A496**, 165 (1989).
[12] Y. Sakuragi, M. Yahiro, and M. Kamimura, Prog. Theor. Phys. Suppl. **89**, 136 (1986).
[13] K. Katori, T. Shimoda, T. Fukuda, S. Shimoura, A. Sakaguchi, M. Tanaka, T. Yamagata, N. Takahashi, H. Ogata, M. Kamimura, and Y. Sakuragi, Nucl. Phys. **A480**, 323 (1988).
[14] Y. Sakuragi, M. Yahiro, M. Kamimura, and M. Tanifuji, Nucl. Phys. **A480**, 361 (1988).
[15] M. Simonius, in *Lecture Notes in Physics*, edited by D. Fick (Springer-Verlag, Heidelberg, 1974), Vol. 30.
[16] P. Zupranski, W. Dreves, P. Egelhof, E. Steffens, D. Fick, and F. Rösel, Nucl. Instrum. Methods **167**, 193 (1979).
[17] *Madison Convention, Proceedings of the 3rd International Symposium on Polarization Phenomena in Nuclear Reactions*, edited by H.H. Barschall and W. Haeberli (University of Wisconsin Press, Madison, 1970).
[18] B.A. Robson, *The Theory of Polarization Phenomena* (Clarendon Press, Oxford, 1974).
[19] D.M. Brink and G.R. Satchler, *Angular Momentum* (Clarendon Press, Oxford, 1979).
[20] P. Zupranski, W. Dreves, P. Egelhof, K.-H. Möbius, E. Steffens, G. Tungate, and D. Fick, Phys. Lett. **91B**, 358 (1980).
[21] A.Y. El-Lithi, computer code, University of Edinburgh (unpublished).
[22] I.J. Thompson, Comput. Phys. Rep. **7**, 167 (1988).
[23] C.M. Perey and F.G. Perey, At. Data Nucl. Data Tables **17**, 1 (1976).
[24] R.P. Ward and P.R. Hayes, At. Data Nucl. Data Tables **49**, 315 (1991).

[25] H.G. Voelk and D. Fick, Nucl. Phys. **A530**, 475 (1991).
[26] K. Rusek, N.M. Clarke, and R.P. Ward, Phys. Rev. C **50**, 2010 (1994).
[27] T. Kajino, Nucl. Phys. **A460**, 559 (1986).
[28] H. Utsunomiya, R.P. Schmitt, Y.-W. Lui, D.R. Haenni, H. Dejbakhsh, L. Cooke, P. Heimberg, A. Ray, T. Tamura, and T. Udagawa, Phys. Lett. B **211**, 24 (1988).
[29] E.W. Macdonald, Monte Carlo computer code UNIMONTE, University of Edinburgh, 1992 (unpublished).
[30] O. Karban, W.C. Hardy, K.A. Connell, S.E. Darden, C.O. Blyth, H.D. Choi, S.J. Hall, S. Roman, and G. Tungate, Nucl. Instrum. Methods A **274**, 4 (1989).
[31] E. Steffens, W. Dreves, P. Egelhof, D. Kasen, W. Weiss, P. Zupranski, and D. Fick, Rev. Phys. Appl. **12**, 1567 (1977).
[32] W. Dreves, H. Jänsch, E. Koch, and D. Fick, Phys. Rev. Lett. **50**, 1759 (1983).
[33] O. Karban, G. Kuburas, C.O. Blyth, H.D. Choi, S.J. Hall, S. Roman, G. Tungate, Z. Moroz, I.M. Turkiewicz, G. Grawert, and N.J. Davis, Nucl. Phys. **A528**, 465 (1991).